Volume 12 | Number 2 | 21 January 2025

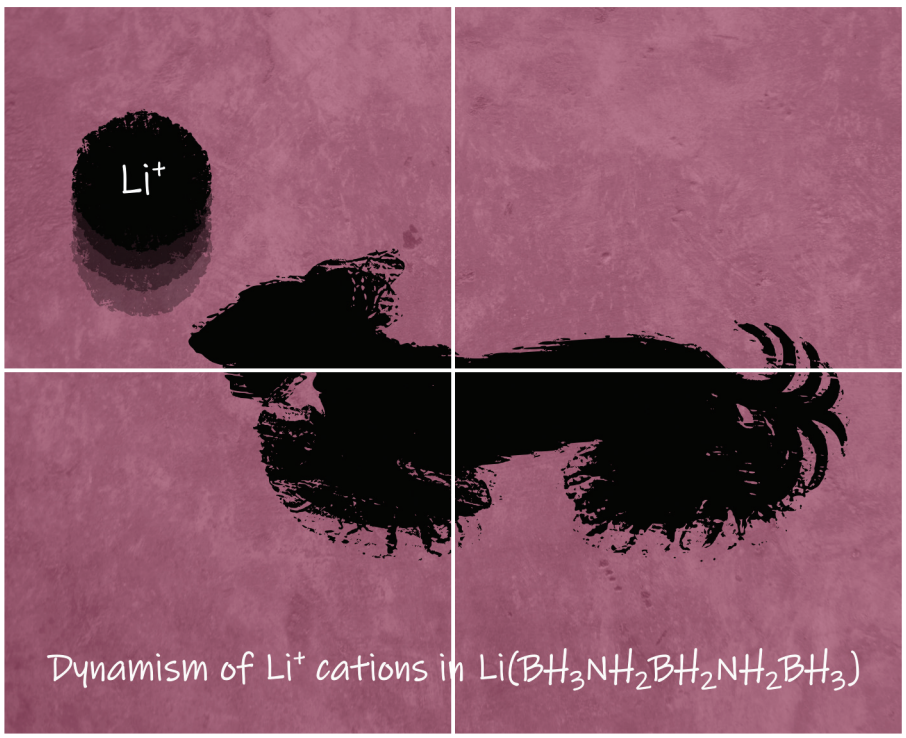

INORGANIC CHEMISTRY

FRONTIERS

CCS 中国化学会 CHINESE CHEMICAL SOCIETY
PEKING UNIVERSITY 1898
ROYAL SOCIETY OF CHEMISTRY
rsc.li/frontiers-inorganic

INORGANIC CHEMISTRY
FRONTIERS

RESEARCH ARTICLE

View Article Online
View Journal | View Issue

Cite this: *Inorg. Chem. Front.*, 2025, **12**, 533

Reinvestigation of the ionic conductivity of a layered $Li(BH_3NH_2BH_2NH_2BH_3)$ salt‡

A. Prus, [a] R. Owarzany, [a] D. Jezierski, [a] M. Rzepecka, [a] W. Grochala, [a] P. Połczyński *[b] and K. J. Fijalkowski *[a]

Received 25th June 2024,
Accepted 14th September 2024

DOI: 10.1039/d4qi01595a

rsc.li/frontiers-inorganic

We reinvestigated the ionic conductivity of lithium ions for $Li(BH_3NH_2BH_2NH_2BH_3)$, an ammonia borane derivative. The observed conductivity (4.0×10^{-6} S cm^{-1} at 65 °C) was found to be over four orders of magnitude higher than the value reported previously at 70 °C for this compound. Since very slow thermal decomposition of $Li(BH_3NH_2BH_2NH_2BH_3)$ progresses already below 100 °C, the previous results reported for 70–130 °C most likely correspond to decomposed samples. The activation energy for the lithium conductivity of polycrystalline layered $Li(BH_3NH_2BH_2NH_2BH_3)$ (57 kJ mol^{-1}) resembles that of powdered Li_3N (59 kJ mol^{-1}), suggesting a similar mechanism of lithium diffusion in both materials.

Introduction

The rapid development of portable electronics and mobile applications has put immense pressure on the development of highly efficient energy storage units. Currently, lithium-ion batteries are preferred owing to their very beneficial large electrical charge-to-mass ratio. However, despite the 40 years development of lithium batteries,[1] safety issues still arise due to flammability and the relatively large mass of the components used.

All types of commercially available lithium-ion batteries use liquid electrolytes to some extent.[2] Organic-solvent-based liquid electrolytes used in Li-ion batteries have numerous advantages (*e.g.* very high lithium solubility and conductivity, excellent wetting properties, and sufficient electric contact with the electrode), but they might be problematic due to flammability when exposed to air, low thermal and electrochemical stability, and poor ionic selectivity.[3] Moreover, organic solvents decrease the effective energy density of the system and promote the formation of dendrites at the surface of lithium electrodes.

The minimisation of the amount of liquid electrolytes used in Li-ion batteries has been one of the hottest research targets in recent years. Systems with an ultra-small volume of electrolytes have been successfully constructed (*e.g.* 10 μL cm^{-2} (ref. 4)); however, the ultimate goal is the construction of an all-solid-state Li-ion battery with no liquid electrolyte, which was first considered as early as the 1950s but was attempted for the first time in the 1990s, followed by numerous successful studies in the 21st century.[5–8] All-solid-state lithium batteries are believed to be lighter, safer, and reach higher capacities than currently used standard batteries; however, issues concerning insufficient cell conductivity at low temperatures and sensitivity to mechanical stress can be expected. None of the studied and constructed all-solid-state lithium-ion batteries are commercially available considering their production problems and relatively high cost. The introduction of such batteries is limited mostly by the inaccessibility of suitable solid electrolyte materials.

Various promising lithium-ion conducting materials were already known in the early 2000s.[9–11] Li-β-alumina ($Li_{20}{\cdot}11Al_2O_3$) with a layered crystal structure facilitating the migration of lithium ions exhibits a conductivity of 1.3×10^{-4} S cm^{-1} at room temperature (RT) but cannot be used as an electrolyte because of its high hygroscopicity.[12] Layered Li_3N shows a very high conductivity of 1.2×10^{-3} S cm^{-1} at RT in the single-crystal form along structural layers but exhibits a low decomposition voltage of 0.44 V.[13–16] LIPON ($Li_{2.88}PO_{3.86}N$) shows good overall properties but suffers from moderate conductivity of only 2×10^{-6} S cm^{-1}, which is insufficient for practical use.[17] In recent years, significant progress has been observed in the field of lithium-ion conducting materials. Currently, $Li_{10}GeP_2S_{12}$ is believed to be the best solid-state candidate for solid electrolyte application, having a conductivity of 1.2×10^{-2} S cm^{-1} but a slightly too narrow electrochemical stability window of 5 V.[18]

Hydride-based materials have also been reported as lithium-ion conductors. $LiBH_4$ exhibits a conductivity of 1×10^{-3} S cm^{-1} after transition to the high-temperature (HT)

[a]*University of Warsaw, Centre of New Technologies, ul. Banacha 2c, 02-097 Warsaw, Poland. E-mail: karol.fijalkowski@cent.uw.edu.pl*
[b]*University of Warsaw, Faculty of Chemistry, ul. Pasteura 1, 02-089 Warsaw, Poland. E-mail: piotrp@chem.uw.edu.pl*

‡Electronic supplementary information (ESI) available: Synthesis, ^{7}Li MAS NMR, Rietveld analysis of Li(B3N2) PXRD, EIS of pristine Li(B3N2). See DOI: https://doi.org/10.1039/d4qi01595a

form above 115 °C, while the low-temperature (LT) form shows a conductivity three orders of magnitude lower.[19] It was subsequently discovered that some doped lithium borohydride materials (*e.g.* $7LiBH_4{\cdot}LiI$;[20] $LiCe(BH_4)_3Cl$ [21]) retain the HT-$LiBH_4$ crystal structure below 115 °C, showing high conductivity at RT (4.5×10^{-5} S cm^{-1};[20] 1.0×10^{-4} S cm^{-1} (ref. 21)).

Protonic-hydridic materials are also known to conduct lithium cations in the solid state. Lithium amidoborane $Li(NH_2BH_3)$ has a relatively poor ionic conductivity of 5.5×10^{-9} S cm^{-1} at RT.[22] However, the adducts of $LiBH_4$ with molecular ammonia borane were reported to show very high conductivity at 40 °C: $(LiBH_4)(NH_3BH_3)$ 4.9×10^{-3} S cm^{-1} and $(LiBH_4)_2(NH_3BH_3)$ 1.2×10^{-4} S cm^{-1}.[23] Recently, Cascallana-Matías *et al.* reported ammonia borane adduct-related materials exhibiting high lithium conductivity at 70 °C: $(LiBH_4)_2(NH_3BH_3)$ 2.83×10^{-5} S cm^{-1}, $(LiI)(NH_3BH_3)$ 1.80×10^{-6} S cm^{-1} and $(LiI)(NH_3BH_3)_2$ 1.79×10^{-5} S cm^{-1}, while $Li(BH_3NH_2BH_2NH_2BH_3)$ had a much poorer conductivity of 4.11×10^{-9} S cm^{-1} at 70 °C.[24] Surprisingly, the figure for $Li(BH_3NH_2BH_2NH_2BH_3)$ was as low as the conductivity of $Li(NH_2BH_3)$ (5.5×10^{-9} S cm^{-1} at RT[22]), having an unfavourable crystal structure with neither the 1D nor 2D lithium cation substructure.

Herein, we present a detailed reinvestigation of the ionic conductivity of $Li(BH_3NH_2BH_2NH_2BH_3)$ performed using an in-house designed IMPED CELL.[25] We present the results of electrochemical impedance spectroscopy (EIS) supported by spectroscopic (FTIR, NMR, Raman, ^{7}Li NMR) and structural (PXRD) studies of the title compound with respect to earlier reports.[24,26,27] We discuss the influences of the chosen synthesis method, the purity of the samples, and the methodology of the solid-state EIS investigation on the material's conductivity.

Results and discussion

$Li(BH_3NH_2BH_2NH_2BH_3)$ (in short: Li[B3N2]) was previously reported by us as a promising hydrogen storage material with a total hydrogen content of 15.2%.[26,27] Its layered crystal structure, with flat sheets of lithium cations separated by thick layers of perpendicularly oriented $(B3N2)^-$ anions,[26] resembles that of Li_3N,[13] a well-known super-ionic lithium conductor.[14–16]

For this study, we have designed a novel approach to the synthesis of Li[B3N2], which is an improvement of the previously reported mechanochemical method.[26] Instead of milling the solid mixture of LiH and NH_3BH_3 in a high-energy mill, we ground the reactants using an agate mortar and pestle to receive an unreacted quasi-homogeneous mixture of the starting compounds, which was further subjected to a 2 hour thermal treatment at 80 °C. The novel method is much easier and more efficient than the classical one[26] and it also avoids the use of metal tools and vessels, ensuring the highest purity of the product received with no electron-conducting metal impurities added upon treatment, which could easily interfere with the results of the EIS investigation. The high purity of

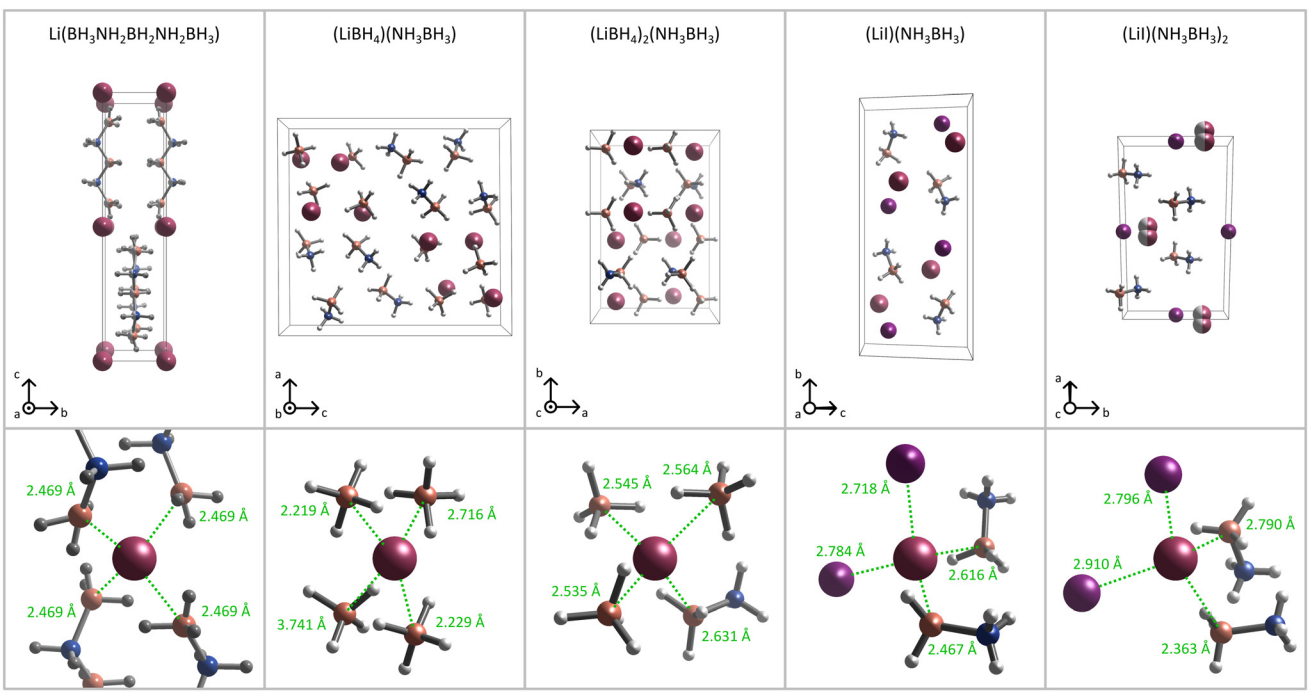

Fig. 1 Top: A comparison of the crystal structures of Li[B3N2],[26] $(LiBH_4)(NH_3BH_3)$,[23] $(LiBH_4)_2(NH_3BH_3)$,[23] $(LiI)(NH_3BH_3)$,[24] and $(LiI)(NH_3BH_3)_2$.[24] Bottom: coordination spheres of lithium cations with Li–B and Li–I distances. For clarity of visualisation, Li coordination spheres are shown with no distortion of $(B3N2)^-$ anions in Li[B3N2][26] and Li^+ cations in $(LiI)(NH_3BH_3)_2$.[24]

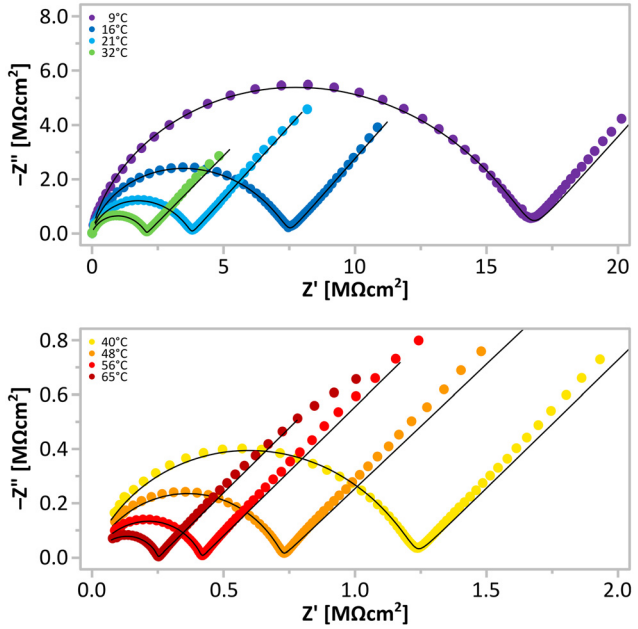

Fig. 2 Nyquist plots of Li[B3N2] recorded in the temperature range of 9–65 °C under 200 MPa, normalised to the electrodes and the effective thickness of the samples in the given conditions and the electrode's area: higher conductivity plots recorded at 40 °C, 48 °C, 56 °C and 65 °C (top) and lower conductivity plots recorded at 9 °C, 16 °C, 21 °C and 32 °C (bottom).

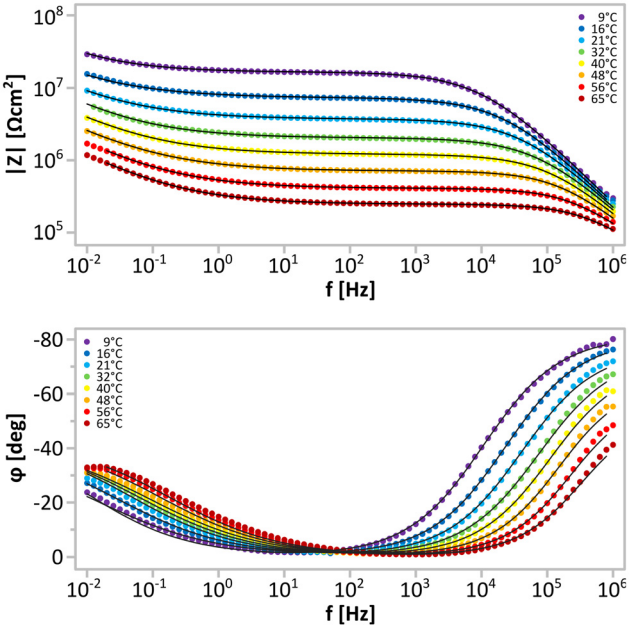

Fig. 3 Bode modulus (top) and Bode phase angle (bottom) plots of Li[B3N2] EIS spectra recorded in the temperature range of 9–65 °C (9 °C, 16 °C, 21 °C, 32 °C, 40 °C, 48 °C, 56 °C, 65 °C) under pressure of 200 MPa, normalised to the samples' effective thickness and the electrode's area.

Li[B3N2] samples obtained *via* the novel method was confirmed by Rietveld analysis§ of its X-ray powder pattern and spectroscopic analyses showing the sole presence of the Li[B3N2] crystalline phase in the product and no contamination with moisture absorbed, which is crucial for the stability of the compound known to be highly hygroscopic.

The EIS measurements were conducted using an in-house developed setup, IMPED CELL.[25] We have acquired several series of temperature-resolved EIS spectra (temperature range of 9–65 °C) for three different batches of Li[B3N2], obtaining consistent results (Fig. 2 and 3). We observed Nyquist plots having shapes of a semicircle followed by spurs at lower frequencies (Fig. 2), typical of materials exhibiting ionic conductivity. The observed semicircles were slightly flattened, similar to the shape of the spectra of related ammonia borane derivatives characterised before.[22] For fitting the spectra, various forms of the dielectric function were tested: Cole–Cole, Davidson–Cole, Jonscher, and Havrilak–Negami. The best quality of the fit was obtained using an equivalent circuit consisting of two branches: one with a single capacitor, and the second with a series connection of Havriliak–Negami and Warburg elements (Fig. 6).[28] The Havriliak–Negami element models ionic relaxation behaviour for the broad and asymmetric distribution of relaxation times characteristic of amorphous materials. The high-frequency capacitance observed at low temperatures takes into account the influence of polymer/anion relaxations at high frequencies.[29] The Warburg element describes diffusive transport mechanisms at low frequencies with charge accumulation at blocking electrodes. The errors of all fitted parameters were below 3%.

We observed the moderate conductivity of Li[B3N2] of 2.6×10^{-7} S cm^{-1} at RT with an activation energy of 57 kJ mol^{-1}, and the expected growth of the material's conductivity at elevated temperatures reached 4.0×10^{-6} S cm^{-1} at 65 °C (Fig. 4 and Table 1). The values at roughly this level of conductivity are characteristic of doped $LiBH_4$ materials exhibiting the HT-$LiBH_4$ crystal structure at lower temperatures.[20]

Surprisingly, the conductivity observed here for polycrystalline Li[B3N2] (2.6×10^{-7} S cm^{-1} at 21 °C, 57 kJ mol^{-1}) is *ca.* fifteen times higher than the conductivity shown by powdered Li_3N (3.7×10^{-8} S cm^{-1} at RT; 59 kJ mol^{-1})[14] having a comparable activation energy, similar layered crystal structure (Table 1) and comparable lithium-lithium distances within the layers (4.020 Å for Li(B3N2),[26] 3.648 Å for Li_3N [13]). This may stem from differences in electrostatic anion–cation interactions. In Li(B3N2), a single negative charge is diluted along the whole $(B3N2)^-$ anion, with partial negative charges localised on nitrogen atoms and hydridic atoms bonded to boron atoms, while in Li_3N a triple-negative charge is localised on nitrogen atoms in Li_2N^- layers, which might inhibit the mobility of Li^+ in lithium. On the other hand, comparable values of conductivity, together with structural similarities of both systems,

§ Obtained Li[B3N2] lattice parameters: a = 4.014 Å, c = 16.924 Å in $P\bar{4}2c$, purity = 99%, GOF = 1.21, R_p = 0.97, wR_p = 1.38.

Table 1 A comparison of lithium ion conductivity parameters of Li[B3N2] and the values reported earlier for Li[B3N2][24] and other relevant hydridic materials: $(LiBH_4)(NH_3BH_3)$,[23] $(LiBH_4)_2(NH_3BH_3)$,[23,24] $(LiI)(NH_3BH_3)$,[24] $(LiI)(NH_3BH_3)_2$,[24] $LiBH_4$,[19] $Li(NH_2BH_3)$,[22] NH_3BH_3 [22] and Li_3N [14–16]

Compound	E_a [kJ mol^{-1}]	σ [S cm^{-1}]	T [°C]	Ref.
$Li(BH_3NH_2BH_2NH_2BH_3)$ – fresh	57	6.0×10^{-8}	9	[Here]
$Li(BH_3NH_2BH_2NH_2BH_3)$ – fresh	57	2.6×10^{-7}	21	[Here]
$Li(BH_3NH_2BH_2NH_2BH_3)$ – fresh	57	4.0×10^{-6}	65	[Here]
$Li(BH_3NH_2BH_2NH_2BH_3)$ – dec.	71	3.0×10^{-9}	25	[Here]
$Li(BH_3NH_2BH_2NH_2BH_3)$ – dec.	71	1.3×10^{-7}	69	[Here]
$Li(BH_3NH_2BH_2NH_2BH_3)$	83	8.7×10^{-9}	70	24
$(LiBH_4)(NH_3BH_3)$	12	4.9×10^{-3}	40	23
$(LiBH_4)_2(NH_3BH_3)$	24	1.2×10^{-4}	40	23
$(LiBH_4)_2(NH_3BH_3)$	69	2.8×10^{-5}	70	24
$(LiI)(NH_3BH_3)$	67	1.8×10^{-6}	70	24
$(LiI)(NH_3BH_3)_2$	46	1.8×10^{-5}	70	24
LT-$LiBH_4$	67	2.0×10^{-8}	25	19
HT-$LiBH_4$	51	1.0×10^{-3}	117	19
$Li(NH_2BH_3)$	140	5.5×10^{-9}	25	22
NH_3BH_3	117	5.2×10^{-11}	60	22
Li_3N (powder)	59	3.7×10^{-8}	25	14
Li_3N (sintered powder)	24	6.6×10^{-4}	25	15
sc-Li_3N (out-of-plane)	47	1.0×10^{-5}	27	16
sc-Li_3N (in-plane)	27	1.2×10^{-3}	27	16

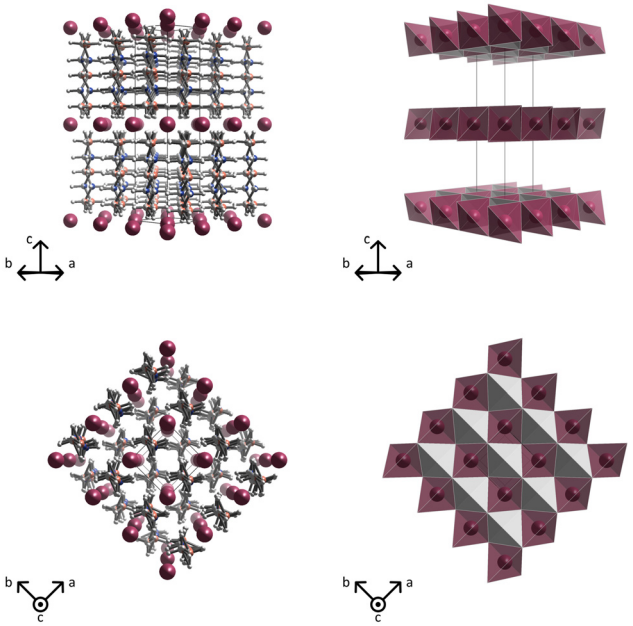

Fig. 5 Visualisations of the crystal structure of Li[B3N2] in the side and top views[26] (left), and the alternating occupied (purple) and vacant (grey) tetragonal sites (T) present within the cationic lithium layers shown in the side and top views (right). Vacant octahedral sites (O) (facing tetragonal sites) are formed on both sides of the cationic layers.

suggest that lithium diffusion in the crystals of Li[B3N2] may resemble the mechanism present in Li_3N,[16] which involves the out-of-plane hopping of Li^+ cations when migrating along the $[Li_2N]^-$ layers in the crystal structure. A closer look at the layered structure of Li[B3N2] revealed that for Li^+ cations to move between the occupied and vacant tetrahedral sites (T) in the lithium layers, they need to pass through out-of-plane octahedral sites (O) (Fig. 5). Such a T–O–T lithium migration pathway is observed in most solid-state lithium conductors that, unfortunately, do not show ultra-high values of conductivity due to the significant energy barrier of crossing the unstable octahedral sites.[30] Numerous similarities between Li[B3N2] and Li_3N also suggest that the conductivity of Li[B3N2] might be several orders of magnitude higher and the activation energy much lower if measured in-plane in single crystals, just as observed for Li_3N (1.2×10^{-3} S cm^{-1} at 27 °C, 27 kJ mol^{-1} (ref. 16)).

The conductivity and activation energy of Li[B3N2] obtained here (4.0×10^{-6} S cm^{-1} at 65 °C, 57 kJ mol^{-1}) significantly differ from the data reported earlier by Cascallana-Matías *et al.*[24] (8.7×10^{-9} S cm^{-1} at 70 °C; 83 kJ mol^{-1}) (Table 1 and Fig. 5). The differences in both conductivity and activation energy are so large that they cannot be simply explained by differences in the measurement setup used or sample quality. Analysis of the results reported by Cascallana-Matías *et al.*[24] led us to conclude that their samples were at least partially thermally decomposed during EIS measurements. Cascallana-Matías *et al.*[24] presented the results of temperature-resolved EIS measurements conducted in the temperature range of *ca.* 70–130 °C (343–403 K), *i.e.*, nominally below the temperature of the thermal decomposition and hydrogen evolution of Li[B3N2] observed at *ca.* 135 °C.[26,27] However, this value was obtained in non-stationary conditions upon dynamic heating,[26,27] while the onset of this process was observed below 100 °C, especially when heated at a low rate.[27] Performing this study, trying to collect data in the temperature range reported in the previous study,[24] we could not obtain stable or reproducible EIS spectra at *ca.* 95 °C, which we believe was a result of the slow decomposition of Li[B3N2]. Thus, Cascallana-Matías *et al.*,[24] while performing their tests at temperatures reaching 130 °C with ≥1 h temperature equilibration, and willing to get reproducible values, must have recorded the data several times in the presented temperature range, effectively decomposing the material. In other words, their conductivity data correspond to at least partially decomposed Li[B3N2].

To check this hypothesis, we subjected a fully thermally decomposed Li[B3N2] sample (1 h at 200 °C under argon) to an EIS study in the temperature range of 13–69 °C. We repeatably obtained the conductivity of 1.3×10^{-7} S cm^{-1} at 69 °C, with an activation energy of 71 kJ mol^{-1}, comparable to the conductivity of LT-$LiBH_4$. These values are still one order of magnitude higher than the figures reported by Cascallana-Matías *et al.*,[24] however, our simple experiment proves that at elevated temperatures Li[B3N2] undergoes substantial chemical changes that adversely affect its electronic conductivity. It should be added here that sample operations reported by Cascallana-Matías *et al.*[24] (the exposure of the sample to air and moisture, presence of platinum paste, heating of a compressed pallet, *etc.*) added so

many uncontrollable factors that it would be surprising if their and our samples (thermally decomposed and measured in inert gas conditions) were not different.

We have also compared the figures obtained for Li[B3N2] with the conductivity reported earlier for ammonia borane-based adducts with LiI and $LiBH_4$.[23,24] We noticed that Li[B3N2] showed similar conductivity to LiI-NH_3BH_3 adducts (Fig. 4) whose crystal structures comprise lithium chains, pseudo-layers, and columns (Fig. 1).[24] Li–Li in-chain distances in $LiI(NH_3BH_3)$ (4.291 Å (ref. 24)) and $LiI(NH_3BH_3)_2$ (4.442 Å (ref. 24)) are only slightly larger than the nearest in-plane distances in Li[B3N2] (4.020 Å (ref. 26)), which is in good agreement with the observed similar conductivities (Tables 1 and 2). Interestingly, lithium chains in $LiI(NH_3BH_3)_2$ lie close to each other, with a Li–Li distance between the chains of just 4.391 Å, forming non-flat pseudo-layers (rendering lithium diffusion easier), while lithium chains in $LiI(NH_3BH_3)$ are well separated from each other, resulting in inferior conductivity.

Li[B3N2] exhibits lower conductivity than $LiBH_4$-NH_3BH_3 adducts[23,24] (Fig. 4), and its crystal structures seem to be more favourable for lithium conductivity. $(LiBH_4)_2(NH_3BH_3)$ is comprised of alternating lithium borohydride ionic layers separated by ammonia borane molecular layers. Lithium cations do not form clear chains or layers, but the Li–Li distances are very short within the lithium borohydride layers (3.417 Å (ref. 30)), and only slightly longer (4.295 Å (ref. 30)) between these layers, which may explain the high conductivity of this material. On the other hand, the crystal structure of $(LiBH_4)(NH_3BH_3)$ consists of borohydride columns separated by regions built exclusively of ammonia borane molecules. Lithium cations do not form straight chains within these columns but rather a network of cations with short interaction distances (3.158–4.363 Å (ref. 33)), while the closest Li–Li distances between the borohydride columns are noticeably longer (5.380 Å (ref. 33)). The high conductivity of $(LiBH_4)(NH_3BH_3)$ can also be explained by the remarkably large volume of the unit cell caused by a substantial share of ammonia borane in the structure. The volume of the unit cell of $(LiBH_4)(NH_3BH_3)$ is 1.4 times larger than the volume of the unit cell of $(LiBH_4)_2(NH_3BH_3)$ (both with $Z = 8$) resulting in an effective decrease in the volume density of lithium cations and this in turn favours high Li-ion conduction.

Table 2 The nearest distances between Li^+ cations observed in lithium planes, chains or columns (Li–Li_{IN}) and between these planes, chains or columns (Li–Li_{OUT}), and the nearest distances between Li^+ cations and boron or iodine atoms in the crystal structure of Li[B3N2] and earlier reported materials[24,26,32–34]

Compound	Li–Li_{IN} [Å]	Li–Li_{OUT} [Å]	Li–X [Å]	Ref.
$Li(BH_3NH_2BH_2NH_2BH_3)$	4.020	8.475	2.469	26
$Li(BH_4)(NH_3BH_3)$	3.158	5.380	2.219	33
$Li(BH_4)_2(NH_3BH_3)$	3.417	4.295	2.535	32
$LiI(NH_3BH_3)$	4.291	6.258	2.467	24
$LiI(NH_3BH_3)_2$	4.420	7.178	2.363	24
LT-$LiBH_4$	3.539	4.271	2.381	34
HT-$LiBH_4$	4.253	4.268	2.474	34

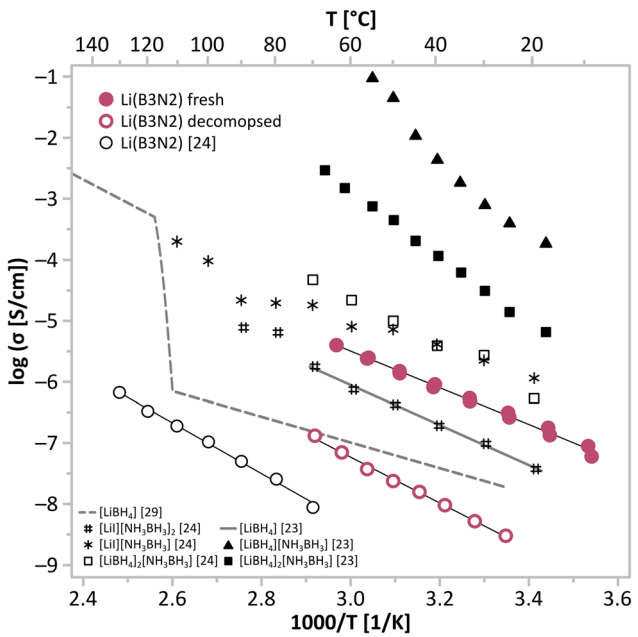

Fig. 4 Comparison of the values of conductivity and activation energy of Li[B3N2] measured in this study (fresh and decomposed at 200 °C) and reported by Cascallana-Matías *et al.*,[24] together with the values characteristic of other ammonia borane-based materials[23,24] and reference values for $LiBH_4$.[23,31]

Conclusions

We have presented a detailed EIS study on the lithium ionic conductivity of Li[B3N2]. The observed conductivity ($\sigma = 4.0 \times 10^{-6}$ S cm^{-1} at 65 °C; $E_a = 57$ kJ mol^{-1}) was found to be significantly higher than the value reported previously for Li[B3N2] (8.7×10^{-9} S cm^{-1} at 70 °C; 83 kJ mol^{-1} (ref. 24)) which is now believed to have shown properties of a thermally decomposed sample. We found that Li[B3N2] undergoes very slow thermal decomposition at *ca.* 95 °C, consistent with earlier thermogravimetric observations.[26,27] This explains why samples of Li[B3N2] studied earlier[24] were largely thermally decomposed, and thus incorrect lithium-ion conductivities were measured for their specimen. Moreover, the conductivity of Li[B3N2] was found to be comparable with that of ammonia borane hybrid adducts with LiI.[24] Surprisingly, polycrystalline Li[B3N2] was found to have a higher conductivity and similar energy barrier for conductivity compared to powdered Li_3N (3.7×10^{-8} at RT; 59 kJ mol^{-1} (ref. 14)). The measurement setup used here (IMPED CELL), allows for the easy and highly precise EIS investigation of air/moisture-sensitive samples of powdered solids.

Experimental

All manipulations were performed under an inert atmosphere of argon (5.0) in an MBRAUN Labmaster DP or Vigor SG1200 glovebox (O_2 < 1.0 ppm; H_2O < 1.0 ppm), avoiding the

use of metal tools and vessels. High-purity reactants were used: NH_3BH_3 (98%, JSC Aviabor), and LiH (95%, Sigma Aldrich).

Synthesis

Li[B3N2] was obtained using a novel method derived from a dry mechanochemical approach reported earlier by us.[26] The entire procedure was carried out without the use of metal tools and vessels to ensure no sample contamination with electronically conducting fractions. LiH and NH_3BH_3 in a molar ratio of 1 : 3 were ground using an agate mortar and pestle for *ca.* 60 seconds until a fine powder was obtained. The as-obtained mixture of starting reactants was heated for 2 h at 75 °C. The process can be described by eqn (1):

$$LiH + 3NH_3BH_3 \rightarrow Li(BH_3NH_2BH_2NH_2BH_3) + NH_3 \uparrow + 2H_2 \uparrow \quad (1)$$

The quality of the product was comparable with the purity of the samples obtained with other known methods[26,27] as judged from PXD, FTIR, and Raman measurements.

Powder X-ray diffraction

PXRD measurements were obtained using a Panalytical X'Pert Pro with linear PIXcel Medipix2 detector (parallel beam; the $CoK_{\alpha 1}$ and $CoK_{\alpha 2}$ radiation intensity ratio of *ca.* 2 : 1, λ ~1.7890 Å). Samples were sealed in 0.5 mm thick quartz capillary tubes under an inert argon atmosphere.

Nuclear magnetic resonance

^{7}Li NMR spectra were obtained using a Bruker AVANCE II 500 MHz spectrometer. $Pb(NO_3)_2$ was used as an intrinsic temperature reference. Due to the risk of explosion (lead nitrate is an oxidant while Li[B3N2] is a reductant), only non-metal tools were used during the sample preparation to avoid sparks. For safety reasons, the temperature range of the measurements was narrowed down to 272–348 K.

Electric impedance spectroscopy

EIS measurements were performed in the frequency range of 10^{-2}–10^{6} Hz using a Solartron 1260A Frequency Response Analyzer with a 1296A Dielectric Interface using the approach reported earlier.[22] All measurements were performed using an in-house designed IMPED CELL[25] available from KEMI (Warsaw, Poland). The IMPED CELL housed the sample under an inert atmosphere (if needed) in an air-tight measurement module that can be loaded inside a glovebox under an inert atmosphere (Fig. 6) with no need for binders or electric contact deposition, enabling the reliable investigation of reactive solids in pure form, which is crucial for moisture sensitive Li(B3N2). The IMPED CELL stabilized the temperature (T ± 0.01 °C) and pressure (p ± 0.1 MPa) with the continuous real-time monitoring of these parameters, together with monitoring the sample's thickness (d ± 1 μm) throughout the entire test, allowing the reliable correction of the results. Each sample (*ca.* 100 mg) was placed inside a sealed stainless-steel

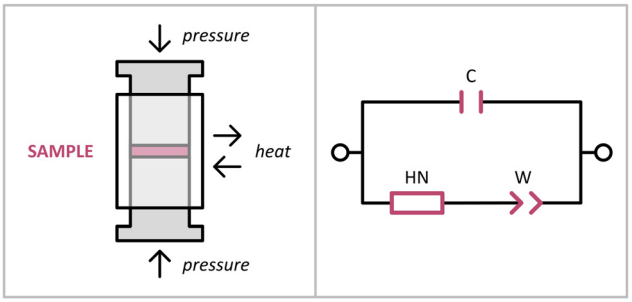

Fig. 6 Scheme of the IMPED CELL showing an air-tight measurement module with the indicated direction of compression and heat exchange (left); the equivalent circuit employs a capacitor (C), Havriliak–Negami (HN) and constant phase element representing the Warburg impedance (W) used for fitting the EIS spectra of Li[B3N2].

module directly between two electrodes (working surface of 0.785 cm^2) and compressed under a pressure of *ca.* 200 MPa during the entire measurement. The temperature was stabilised with a dedicated water jacket coupled with a Lauda RE 1050 thermostat and controlled *via* SMART software from Solartron. The pressure was stabilised using a SPECAC ATLAS 15T laboratory press. The sample thickness was monitored using a SICK OD Mini LIDAR distance sensor. All the auxiliary data (T, p, d) were collected and synchronised using a dedicated data acquisition unit. The IMPED CELL was loaded under argon gas inside the glovebox. Each experimental spectrum was measured until the value was reproduced. Fitting was carried out using the ZPlot software from Scribner Associates, Inc.

The **IMPED CELL** was designed to provide a versatile, user-friendly tool for EIS research. The development was performed under the Stanford Design Thinking Model approach with a functional usability study based on qualitative analysis employing in-depth interviews and mini-focus group workshops with participants representing the International Electrochemical Society.

Graphical presentation

Visualisations of crystal structures have been performed with Vesta.[35] Illustrations have been prepared using Inkscape 0.92.1.[36]

Data availability

The data supporting this article have been included as part of the ESI.‡

Conflicts of interest

There are no conflicts to declare.

Acknowledgements

This research was funded by Polish National Science Centre within the projects Sonata Bis 8 (UMO/2018/30/E/ST5/00854) and Preludium 13 (UMO/2017/25/N/ST5/01977). Development and prototyping of IMPED CELL was funded by Polish National Centre for Research and Development within the project Tango 2 (TANGO2/340584/NCBR/2017). The authors thank all the participants of the functional usability study from Cambridge in the UK, Belgrade in Serbia, and Warsaw in Poland. The authors thank Mr Krzysztof Dawid (KEMI, Warsaw, Poland) for his support in the development of IMPED CELL. The research was carried out with the use of CePT infrastructure financed by the European Union – the European Regional Development Fund within the Operational Programme "Innovative economy" for 2007–2013 (POIG.02.02.00-14-024/08-00). This work is dedicated to Prof. Zbigniew Galus at his 90th birthday.

References

1 M. S. Whittingham, Electrical energy storage and intercalation chemistry, *Science*, 1976, **192**, 1126–1127.
2 J. M. Tarascon and M. Armand, Issues and challenges facing rechargeable lithium batteries, *Nature*, 2001, **414**, 359–367.
3 E. Quartarone and P. Mustarelli, Electrolytes for solid-state lithium rechargeable batteries: recent advances and perspectives, *Chem. Soc. Rev.*, 2011, **40**, 2525–2540.
4 B. Hamankiewicz, A. Czerwiński, M. Krajewski, M. Michalska, L. Lipińska, J. Kozakiewicz, J. Przybylski, K. Sylwestrzak and W. Sarna, Lithium-ion cel, *Polish patent application no P.*416704, 2016.
5 K. Iwamoto, N. Aotani, K. Takada and S. Kondo, Application of Li_3PO_4-L_2S-SiS_2 glass to the solid state secondary batteries, *Solid State Ionics*, 1995, **79**, 288–291.
6 Y. Kato, S. Hori, T. Saito, K. Suzuki, M. Hirayama, A. Mitsu, M. Yonemura, H. Iba and R. Kanno, High-power all-solid-state batteries using sulphide superionic conductors, *Nat. Energy*, 2016, **1**, 16030.
7 T. Takeuchi, H. Kageyama, K. Nakanish, M. Tabuchi, H. Sakaebe, T. Ohta, H. Senoh, T. Sakai and K. Tatsumi, All-Solid-State Lithium Secondary Battery with Li_2S-C Composite Positive Electrode Prepared by Spark-Plasma-Sintering Process, *J. Electrochem. Soc.*, 2010, **157**, A1196–A1201.
8 K. Yoon, J. J. Kim, W. M. Seong, M. H. Lee and K. Kang, Investigation on the interface between $Li_{10}GeP_2S_{12}$ electrolyte and carbon conductive agents in allsolid-state lithium battery, *Sci. Rep.*, 2018, **8**, 8066.
9 V. Thangadurai and W. Weppner, Recent progress in solid oxide and lithium ion conducting electrolytes research, *Ionics*, 2016, **12**, 81–92.
10 S. Stramare, V. Thangadurai and W. Weppner, Lithium Lanthanum Titanates: A Review, *Chem. Mater.*, 2003, **15**, 3974–3990.
11 V. Thangadurai, H. Kaack and W. Weepner, Novel Fast Lithium Ion Conduction in Garnet-Type $Li_5La_3M_2O_{12}$ (M = Nb, Ta), *J. Am. Ceram. Soc.*, 2003, **86**, 437.
12 J. L. Briant and G. C. Farrington, Ionic Conductivity in Lithium and Lithium-Sodium Beta Alumina, *J. Electrochem. Soc.*, 1981, **128**, 1830–1934.
13 A. Rabenau and H. Schulz, Re-evaluation of the lithium nitride structure, *J. Less-Common Met.*, 1976, **50**, 155–159.
14 B. A. Boukamp and R. A. Huggins, Lithium ion conductivity in lithium nitride, *Phys. Lett. A*, 1976, **58**, 231–233.
15 B. A. Boukamp and R. A. Huggins, Fast ionic conductivity in lithium nitride, *Mater. Res. Bull.*, 1978, **13**, 23–32.
16 U. v. Alpen, A. Rabenau and G. H. Talat, Ionic conductivity in Li_3N single crystals, *Appl. Phys. Lett.*, 1977, **30**, 621–623.
17 J. B. Bates, N. J. Dudney, G. R. Gruzalski, R. A. Zuhr, A. Choudhury, C. F. Luck and J. D. Robertson, Electrical properties of amorphous lithium electrolyte thin films, *Solid State Ionics*, 1992, **53–56**, 647–654.
18 N. Kamaya, K. Homma, Y. Yamakawa, M. Hirayama, R. Kanno, M. Yonemura, T. Kamiyama, Y. Kato, S. Hama, K. Kawamoto and A. Mitsui, A lithium superionic conductor, *Nat. Mater.*, 2011, **10**, 682–686.
19 M. Matsuo, Y. Nakamori, S. Orimo, H. Maekawa and H. Takamura, Lithium superionic conduction in lithium borohydride accompanied by structural transition, *Appl. Phys. Lett.*, 2007, **91**, 224103.
20 H. Maekawa, M. Matsuo, H. Takamura, M. Ando, Y. Noda, T. Karahashi and S. I. Orimo, Halide-Stabilized $LiBH_4$, a Room-Temperature Lithium Fast-Ion Conductor, *J. Am. Chem. Soc.*, 2009, **131**, 894–895.
21 M. B. Ley, D. B. Ravnsbek, Y. Filinchuk, Y. S. Lee, R. Janot, Y. W. Cho, J. Skibsted and T. R. Jensen, $LiCe(BH_4)_3Cl$, a New Lithium-Ion Conductor and Hydrogen Storage Material with Isolated Tetranuclear Anionic Clusters, *Chem. Mater.*, 2012, **24**, 1654–1663.
22 K. J. Fijalkowski, R. Jurczakowski, W. Koźmiński and W. Grochala, Insights from impedance spectroscopy into the mechanism of thermal decomposition of $M(NH_2BH_3)$, M = H, Li, Na, $Li_{0.5}Na_{0.5}$, hydrogen stores, *Phys. Chem. Chem. Phys.*, 2012, **14**, 5778–5784.
23 H. Liu, Z. Ren, X. Zhang, J. Hu, M. Gao, H. Pan and Y. Liu, Incorporation of Ammonia Borane Groups in the Lithium Borohydride Structure Enables Ultrafast Lithium Ion Conductivity at Room Temperature for Solid-State Batteries, *Chem. Mater.*, 2020, **32**, 671–678.
24 I. Cascallana-Matías, J. Breternitz, A. Baker, H. Davis, E. J. Cussen and D. H. Gregory, Molecular-salt hybrids; integration of ammonia borane into lithium halides, *Inorg. Chem. Front.*, 2019, **6**, 808–812.
25 K. J. Fijalkowski and R. Jurczakowski, Cell and method for electrical measurements of highly reactive powder and liquid samples, Patents no. PL221643 (2016), EP2788745 (2016), US9651595 (2017), JP6219831 (2017).
26 K. J. Fijalkowski, T. Jaroń, P. J. Leszczyński, E. Magoś-Palasyuk, T. Palasyuk, M. K. Cyrański and W. Grochala, M $(BH_3NH_2BH_2NH_2BH_3)$ – the missing link in the mecha-

nism of the thermal decomposition of light alkali metal amidoboranes, *Phys. Chem. Chem. Phys.*, 2014, **16**, 23340–23346.

27 R. Owarzany, K. J. Fijałkowski, T. Jaroń, P. J. Leszczyński, Ł. Dobrzycki, M. K. Cyrański and W. Grochala, Complete Series of Alkali-Metal M($BH_3NH_2BH_2NH_2BH_3$) Hydrogen-Storage Salts Accessed via Metathesis in Organic Solvents, *Inorg. Chem.*, 2016, **55**, 37–45.

28 J. R. Dygas, Dielectric function of ionic conductors studied by impedance spectroscopy, *Solid State Ionics*, 2005, **176**, 2065–2078.

29 I. B. Pehlivan, R. Marsal, P. Georén, C. G. Granqvist and G. A. Niklasson, Ionic relaxation in polyethyleneimine-lithium bis (trifluoromethylsulfonyl) imide polymer electrolytes, *J. Appl. Phys.*, 2010, **108**, 074102.

30 Y. Wang, W. D. Richards, S. P. Ong, L. J. Miara, J. C. Kim, Y. Mo and G. Ceder, Design principles for solid-state lithium superionic conductors, *Nat. Mater.*, 2015, **14**, 1026–1032.

31 D. Sveinbjornsson, J. S. G. Myrdal, D. Blanchard, J. J. Bentzen, T. Hirata, M. B. Mogensen, P. Norby, S. I. Orimo and T. Vegge, Effect of Heat Treatment on the Lithium Ion Conduction of the $LiBH_4$–LiI Solid Solution, *J. Phys. Chem. C*, 2013, **117**, 3249–3257.

32 H. Wu, W. Zhou, F. E. Pinkerton, M. S. Meyer, G. Srinivas, T. Yildirim, T. J. Udovic and J. J. Rush, A new family of metal borohydride ammonia borane complexes: Synthesis, structures, and hydrogen storage properties, *J. Mater. Chem.*, 2010, **20**, 6550–6556.

33 J. Luo, H. Wub, W. Zhou, X. Kang, Z. Fang and P. Wang, $LiBH_4{\cdot}NH_3BH_3$: A new lithium borohydride ammonia borane compound with a novel structure and favorable hydrogen storage properties, *Int. J. Hydrogen Energy*, 2012, **37**, 10750–10757.

34 Y. Filinchuk, D. Chernyshov and R. Cerny, Lightest Borohydride Probed by Synchrotron X-ray Diffraction: Experiment Calls for a New Theoretical Revision, *J. Phys. Chem. C*, 2008, **112**, 10579–10584.

35 K. Momma and F. Izumi, VESTA 3 for three-dimensional visualization of crystal, volumetric and morphology data, *J. Appl. Crystallogr.*, 2011, **44**, 1272–1276.

36 Inkscape project, 2017.